

Class B Sodalites: Nonstoichiometric Silver,Sodium Halosodalites

Andreas Stein,[†] Geoffrey A. Ozin,^{*†} and Galen D. Stucky[‡]

Contribution from the Lash Miller Chemical Laboratories, University of Toronto, 80 Saint George Street, Toronto, Ontario, Canada, M5S 1A1, and Department of Chemistry, University of California, Santa Barbara, California 93106. Received January 27, 1992

Abstract: Nonstoichiometric silver,sodium bromosodalites of the compositions $M_{8-2n}N_{2n}X_{2-p}OH_p$ -SOD and $M_{8-2n}N_{2n}X_{2-p}[\]_p$ -SOD have been synthesized, where $M, N = Ag^+, Na^+, X = Cl^-, Br^-, I^-, 2n = 0-8, p = 0-2, [\]$ refers to anion-free cages and SOD = $(SiAlO_4)_6^{6-}$. These materials allow one to control the filling of both Ag^+ and X^- ions in a sodalite host lattice in a systematic manner to fabricate $Na_{4-n}Ag_nX$ semiconductor-component clusters. Combined results from powder XRD, Rietveld refinement, ^{23}Na MAS and DOR NMR, and far-IR and mid-IR spectroscopy indicate that these sodalites form a solid solution of $Na_{3-m}Ag_m$ clusters in anion-free β -cages interspersed with $Na_{4-n}Ag_nX$ clusters. The clusters are statistically distributed throughout the lattice. However, silver ions are associated preferentially with cavities containing halide anions. The data also demonstrate that these materials offer the opportunity to manipulate the extent of collective electronic and vibrational interactions between monodispersed $Na_{4-n}Ag_nBr$ clusters in a perfectly crystalline host. The anion strongly mediates the vibrational coupling. The electronic coupling between clusters increases with Ag^+ and X^- loading levels. Support for this idea comes from extended Hückel molecular orbital calculations. At low Ag^+/X^- loadings, intrasodalite AgX resembles the gas-phase molecule (bond length, optical spectra). Optical absorption bands broaden and the absorption edge moves toward that of the bulk semiconductor at higher Ag^+/X^- loadings.

Introduction

Recently we have shown^{1,2} that class A silver,sodium halosodalites allow the atomically precise assembly of I-VII semiconductor components in a sodalite lattice. By tuning the silver concentration it was possible to cover the range from silver bromide exhibiting molecular behavior at low silver loadings to an expanded silver bromide supralattice at complete silver exchange.¹ In this paper a series of novel silver,sodium halohydroxosodalites of the type $Na_{8-p-2n}Ag_{2n}X_{2-p}[\]_p$ -SOD, where SOD = $Si_6Al_6O_{24}$, $[\]$ = an anion-free cage, $p = 0-2$, and $2n = 0-8$, will be discussed which are derived from sodium halohydroxosodalites of the type $Na_8X_{2-p}(OH)_p$ -SOD.³ In these materials, single-size $Na_{4-n}Ag_nX$ ($n = 0-4$) clusters are dispersed within a perfectly periodic array of all-space-filling β -cages, but in contrast to the previously described sodalites (class A, class C),^{1,2,4} they are isolated from each other by sodalite cages containing no anion, forming a class B supralattice of nonstoichiometric⁵ silver,sodium halosodalite. The anion-free cages are filled with $Na_{3-n}Ag_n$ ($n = 0-3$) triangles, and in the hydrated form with water molecules. Denks⁵ has defined a nonstoichiometric sodalite as a solid-phase solution of NaX -SOD and $Na[\]$ -SOD, in which overall β -cavities with sodalitic and zeolitic fillings are statistically interspersed. Our definition of class B sodalites also includes sodalites containing nonstoichiometric amounts of other anions, including the oxalates⁶ and the halates recently prepared by Hund and Geismar ($Na_8X_{2-p}(OH)_p$ -SOD, $X = ClO_3, BrO_3, ClO_4$),⁷ as well as their silver derivatives. The end members for the $p = 2$, nonbasic hydroxosodalite ($Na[\]$ -SOD), hydroxosodalite (NaOH-SOD, basic hydroxosodalite), are considered in this paper as special cases of class B sodalites. The other end members of the series with $p = 0$ are really class A sodalites. The hydrated forms of class B sodalites contain additional water molecules, e.g., in zeolite Zh = $Na[\]$ -SOD up to four water molecules per β -cage and in NaOH-SOD one water molecule per cavity⁸ (up to two water molecules according to Ernst et al. and Felsche et al.^{9,10} and up to three according to Denks⁵). As water can pass through the sodalite six-rings, these framework aluminosilicates can be classified as zeolites.⁵

For class A sodalites it has been shown that orbital overlap and electronic/vibrational communication are possible between clusters in adjacent cages and therefore throughout the lattice. In class B sodalites on the other hand, cages lacking an anion break the

Table I. Gel Compositions for Sodalite Syntheses^a

product	xAl(OH) ₃	ySiO ₂	zNaOH	vH ₂ O	wNaX	salt
NaOH-SOD BrL0	1	1	5	41	0	
NaBrOH-SOD BrLI	1	1	5	41	0.070	NaBr
NaBrOH-SOD BrLII	1	1	5	41	0.0135	NaBr
NaBrOH-SOD BrLIII	1	1	5	41	0.20	NaBr
NaBrOH-SOD BrLA	1	1	5	41	0.625	NaBr
NaBrOH-SOD BrLB	1	1	5	41	0.94	NaBr
NaBr-SOD BrLF	1	2	8	100	5	NaBr
NaIOH-SOD ILI	1	1	5	41	0.070	NaI

^a All values are given in moles, relative to 1 mole of Al(OH)₃.

periodicity between Ag_4X^{3+} clusters. This effect can change cooperative effects between clusters, which require the presence of a halide atom (vibrational) or its orbitals (electronic). For a solid solution, variations in the halide content, p , are expected to alter the mean distance between $Na_{4-n}Ag_nX$ clusters, while changes in the silver content, n , and thus the sodium:silver ratio, shift the constituents of the clusters from those of an insulator to a semiconductor type. At low halide and silver concentrations, isolated AgX molecules may be produced in class B materials. Such controlled tunable volume filling and compositional alteration of the contents of the sodalite β -cages provide an unprecedented opportunity to adjust the extent of electronic and vibrational

(1) Stein, A.; Ozin, G. A.; Stucky, G. D. *J. Am. Chem. Soc.* **1990**, *112*, 904-905.

(2) Stein, A.; Ozin, G. A.; Macdonald, P. M.; Stucky, G. D.; Jelinek, R. *J. Am. Chem. Soc.* **1992**, *114*, 5171-5186.

(3) Stein, A.; Macdonald, P. M.; Stucky, G. D. *J. Phys. Chem.* **1990**, *94*, 6943-6948.

(4) Stein, A.; Meszaros, M.; Macdonald, P. M.; Ozin, G. A.; Stucky, G. D. *Adv. Mater.* **1991**, *3*, 306-309.

(5) Denks, V. P. *Tr. Inst. Fiz. Akad. Nauk Est. SSR* **1984**, *55*, 14-71.

(6) Stein, A.; Ozin, G. A.; Stucky, G. D. *J. Soc. Photogr. Sci. Technol. Jpn.* **1990**, *53*, 322-328.

(7) Hund, F.; Geismar, G. *Chem.-Ztg.* **1990**, *114*, 243-244.

(8) Hassan, I.; Grundy, H. D. *Acta Crystallogr.* **1983**, *C39*, 3-5.

(9) Ernst, H.; Pfeifer, H.; Zhdanov, S. P. *Zeolites* **1983**, *3*, 209-213.

(10) Felsche, J.; Luger, S. *Ber. Bunsenges. Phys. Chem.* **1986**, *90*, 731.

[†] University of Toronto.

[‡] University of California.

Table II. List of Reagents for Sodalite Synthesis and Silver Exchange

Al(OH) ₃	Fisher, 99.8%
SiO ₂	Ludox HS-30, Ludox HS-40 (Du Pont), Luddy (40%, Alchem) (colloidal aqueous silica sources)
NaOH	Mallinckrodt, 98.7%
H ₂ O	deionized
NaBr	Mallinckrodt, 99.0%
NaI	BDH, 99.0%
AgNO ₃	Fisher, 99.8%
NaNO ₃	Fisher, certified ACS grade

coupling between fixed nuclearity Na_{4-n}Ag_nX clusters. It should therefore be possible to chemically manipulate the electronic band structure of the materials and thus their electronic and optical properties. The synthetic details and structural, vibrational, magnetic resonance, and optical properties of the class B sodalites will be addressed in this paper.

Synthesis

Synthesis of Sodium Sodalite Precursors. The sodium sodalites were prepared by a low-temperature hydrothermal synthesis. The gel compositions are listed in Table I and the reagent sources in Table II. In a typical synthesis, solution A contained the sodium salt, sodium hydroxide, and silica source, and solution B contained sodium hydroxide and the alumina source. These were prepared as follows. For solution A, (0.6)(z) mol of NaOH and w mol of the sodium salt to be occluded in the sodalite were dissolved in (0.6)(v) mol of deionized water. An aqueous colloidal silica solution containing y mol of SiO₂ was added to the above solution. The solution was mixed and heated to 80–95 °C. Solution B was prepared by dissolving x mol of Al(OH)₃ in an aqueous solution containing (0.4)(z) mol of the NaOH, again at 80–95 °C. The hot solutions A and B were mixed rapidly. A gel formed almost immediately upon mixing. The gel was shaken for 5 min, and the mixture was heated at 95 °C for 3–9 days in 1000-mL capped teflon (FEP) bottles. The white, microcrystalline products were filtered through ASTM 10–15 medium pore glass frits and washed with 2–4 L of deionized water. The products were dried in air at ambient temperature.

Soxhlet Extraction. Sodium hydroxosodalites and sodalites containing hydroxide in addition to halide anions were Soxhlet extracted to remove one NaOH molecule per β-cage. The hydroxide ion is the only anion small enough to pass through the sodalite six-rings at room temperature. About 15 g of sodalite was placed in a thimble and continuously refluxed for 3 days in a Soxhlet extraction apparatus with 500 mL of deionized water. Concentrated H₂SO₄ (2 mL) had been added to the water to prevent foaming and improve the extraction efficiency.

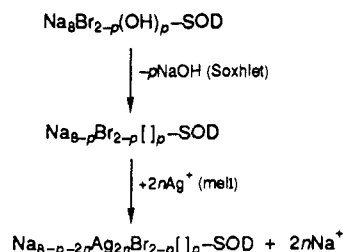
Silver Exchange. Melt Exchange. Silver-containing sodalites were prepared by a melt ion exchange of a mixture containing the parent sodium sodalite, AgNO₃ (Fisher, 99.8%), and in some cases NaNO₃ (ACS grade) as diluent. Typically, 1–2 g of sodium sodalite was mixed with silver nitrate (mp 212 °C) in a porcelain mortar. For complete silver exchange a slight excess of silver nitrate was used, while for partial exchanges stoichiometric amounts were used. The mixture was heated in the dark to 230 °C for 24 h (320 °C if NaNO₃ was used). The products were filtered in the dark through a 0.8-μm cellulose nitrate filter membrane, washed with ca. 2 L of deionized water, and dried in air at ambient temperature. Because of their light sensitivity, the white-to-yellow dry powders were stored in dark sample vials.

Aqueous Exchange. An aqueous ion exchange is possible for even milder exchange temperatures (room temperature up to 100 °C). Sodium sodalite was added to an aqueous solution containing stoichiometric amounts of silver nitrate. The mixture was stirred in the dark for 24 h at room temperature. The product was filtered, washed in the dark, and dried in air. Analysis by far-infrared spectroscopy showed that replacement of sodium by silver had proceeded to completion or nearly so.

Dehydration. The sodium sodalites were dehydrated under vacuum (10⁻⁴–10⁻⁶ Torr) by the following temperature ramps: room temperature to 100 °C in 30 min, held at 100 °C for 1 h, 100–450 °C (or 550 °C) over 4 h, and then held isothermally at 450 °C (or 550 °C) for 1 h. Since Ag⁺ ions are easily reduced, sometimes even after pumping, samples containing Ag⁺ were heated to 100 °C much more slowly, held at that temperature for a longer time, and heated to a lower maximum temperature (ca. 300–450 °C) than sodium sodalites. Dehydration of relatively open sodalite systems (those containing anion-free cages) occurred at considerably lower temperatures (ca. 100 °C lower) than for sodalites in which all cages were filled with anions. In the latter, all of the (111) channels are blocked by Na⁺ ions, and it is only after partial removal of the Na⁺ ions from the centers of the 6-membered windows that it be-

comes possible for the water molecules to leave.⁵

The product crystallinity was monitored by powder XRD at each step. The reactions are summarized in the following scheme:



Details of the chemical analyses, powder XRD, Rietveld refinement, ²³Na MAS and DOR NMR, far-IR, mid-IR, and optical reflectance spectroscopy, and extended Hückel molecular orbital calculations have been recently described.²

Product Characterization

Chemical Analysis. Samples containing various substoichiometric amounts of halide have been synthesized with the silver loading varied over the whole range of 2n = 0–8. A chemical analysis (Table III) showed that the products obtained from the hydrothermal synthesis consisted of both Na₄OH and Na₄Br occupied cages and that the amount of halide included in the hydroxosodalites was generally much lower than the amount added to the reaction vessel. The isotherm for bromosodalite favors the inclusion of bromide over hydroxide or water.¹¹ However, as for most sodalites, excess salt is required to form a product in which all cages are filled with monovalent anions. Otherwise, the sodalites contain cages with imbibed hydroxide or water, or completely different phases such as cancrinite can be created.¹¹

The bromide concentrations were virtually identical for a sodalite before and after Soxhlet extraction. Because of their size (r(Br⁻) = 1.82 Å, C.N. 6),¹² bromide ions were not washed out through the sodalite six-rings (r = 1.10–1.30 Å),¹³ and their distribution throughout the sodalite lattice could not change after the hydrothermal synthesis.

The sodium aggregates could be progressively exchanged by silver ions to yield at full substitution the corresponding mixture of (2 - p)Ag₄Br and pAg₃ units. A single sodalite phase was observed for a given bulk composition by powder XRD in fully hydrated samples after each reaction step. In a completely silver-exchanged sample containing Br⁻ in one out of eight cages, less than 0.9 mol % Na was found by chemical analysis after aqueous exchange.

Powder XRD Unit Cell Dimensions. Knowledge of the effect of the sodalite composition on the unit cell size and the interatomic distances is vital to understanding the coupling between atoms and thus the electronic and optical properties of the materials. The unit cell sizes of the class B sodalites studied are listed in Table IV. The edge lengths of the cubic unit cell depended on the silver and bromide concentrations as well as on the degree of hydration. The response of the sodalite framework to the gradual addition of Br⁻ anions to the unit cell of Na[]-SOD, eventually yielding NaBr-SOD, is shown for the fully hydrated samples in Figure 1. The interpretation of the unit cell data requires an appreciation of the role of imbibed water. Neutron diffraction studies on Na[]-SOD·nH₂O (n = 0,8)^{10,14} demonstrate that the water molecules are both coordinated to the Na⁺ six-ring cations and hydrogen-bonded to the framework oxygens. The first Br⁻ entering the Na₃ cages to form Na₄Br clusters causes the unit cell to expand (partial loss of structural hydrogen bonding from β-cage imbibed H₂O), while the further influx of Br⁻ up to full loading has a cage contraction effect (electrostatic attraction by Na₄Br formation) as seen by the gradual diminution of the sodalite unit cell dimension. Upon dehydration the unit cells of these samples expand,

(11) Barrer, R. M. *Hydrothermal Chemistry of Zeolites*; Academic Press: London, 1982.

(12) Shannon, R. D. *Acta Crystallogr.* 1976, A32, 751–767.

(13) Breck, D. W. *Zeolite Molecular Sieves*; R. E. Kieger Publishing Company: Malabar, 1984.

(14) Felsche, J.; Luger, S.; Baerlocher, C. *Zeolites* 1986, 6, 367–372.

Table III. Compositions of Class B Sodalites

Chemical Analysis										
sample ^a	%Na	%Ag	%Br	%Si	%Al	%O	ppm Fe	Si/Al	composition	tot. M ⁺ /uc
Na[]-SOD BrL0	14.73	0.00	0.00	20.25	18.98	46.02	160	1.02	Na _{5.46} Si _{6.07} Al _{5.93} O _{24.2}	5.40
NaBr[]-SOD BrLI ^b	14.39	0.00	2.39	19.68	18.42	45.11	130	1.03	Na _{4.39} Na _{1.04} Br _{0.26} Si _{6.08} Al _{5.92} O _{24.4}	5.43
NaBr[]-SOD BrLII	14.76	0.00	4.28	19.99	18.60	42.36	110	1.03	Na _{3.66} Na _{1.84} Br _{0.46} Si _{6.10} Al _{5.90} O _{22.7}	5.50
NaBrOH-SOD BrLI	16.68	0.00	2.45	18.74	17.87	44.24	160	1.01	Na _{5.44} OH ₂ Na _{1.11} Br _{0.28} Si _{6.02} Al _{5.98} O _{25.0}	6.55
AgBr[]-SOD BrLI ^b	0.115	40.84	1.86	11.06	10.87	35.26	4420	0.98	Ag _{4.3} Ag _{1.4} Br _{0.35} Si _{5.93} Al _{6.07} O _{33.2}	5.70
NaBr-SOD BrLF	16.27	0.00	13.70	16.17	15.03	38.83	47	1.03	Na _{7.50} Br _{1.82} Si _{6.10} Al _{5.90} O _{25.7}	7.50

Neutron Activation Results			
sample ^c	composition	tot. Na/uc	feed Br/uc
Na[]-SOD BrL0	Na _{5.73} -SOD	5.73	0.00
NaBr[]-SOD BrLI	Na _{4.64} Na _{1.16} Br _{0.29} -SOD	5.80	0.42
NaBr[]-SOD BrLII	Na _{3.95} Na _{2.1} Br _{0.53} -SOD	6.05	0.81
NaBr[]-SOD BrLIII	Na _{1.94} Na _{4.72} Br _{1.18} -SOD	6.66	1.2
NaBr[]-SOD BrLA	Na _{1.17} Na _{5.56} Br _{1.39} -SOD	6.73	3.8
NaBr[]-SOD BrLB	Na _{0.94} Na _{6.52} Br _{1.63} -SOD	7.46	5.6
NaBr-SOD BrLF	Na _{7.36} Br _{1.63} -SOD	7.36	7.5
NaOH-SOD BrL0	Na _{6.57} OH ₂ -SOD	6.57	0.00
NaBrOH-SOD BrLI	Na _{5.57} OH ₂ Na _{1.16} Br _{0.29} -SOD	6.73	0.42
NaBrOH-SOD BrLII	Na _{4.66} OH ₂ Na _{2.04} Br _{0.51} -SOD	6.70	0.81
NaBrOH-SOD BrLIII	Na _{2.22} OH ₂ Na _{5.16} Br _{1.29} -SOD	7.38	1.2
NaBrOH-SOD BrLA	Na _{1.93} OH ₂ Na _{5.76} Br _{1.44} -SOD	7.69	3.8

^a Samples were dehydrated under vacuum at 500 °C for 1 h. ^b Water of hydration (nonsurface) in the hydrated sample: NaBr[]-SOD BrLI, 5.9%; AgBr[]-SOD BrLI, 4.7%. ^c Samples were hydrated. Feed Br/uc is the expected bromide concentration from the feed composition, assuming all bromide present in the reagents enters the product.

Table IV. Unit Cell Sizes (Å) of Class B Sodalites^a

Br loading (Br/uc)	Ag loading (Ag/uc)						
	0	0.1	1	2	4	8	dehydrated 0
NaAgBr[]-SOD							
0.00	8.854 (3)	8.963 (2) ^b	8.959 (2)	8.969 (2)		8.975 (4)	9.092 (2)
0.26	8.972 (3)	8.965 (1)	8.957 (3)	8.954 (2)		8.966 (2)	9.053 (3)
0.46	8.964 (4)	8.964 (2)	8.956 (3)	8.955 (2)		8.955 (3)	9.019 (2)
1.18	8.948 (1)	8.946 (1)	8.943 (1)	8.936 (2)		8.938 (2)	8.959 (1)
1.82	8.927 (3)		8.924 (3)			8.906 (2)	8.958 (4)
NaAgBrOH-SOD							
0.00	8.902 (3)	8.964 (2) ^c	8.959 (2)			8.949 (3)	8.7342 (8) ^e
0.29	8.916 (3)						
0.53	8.920 (3)						
1.18	8.933 (2)	8.943 (2)	8.936 (2)	8.929 (2)		8.931 (3)	
1.82	8.927 (3)		8.924 (3)			8.906 (2)	
NaAgI[]-SOD ILI							
	8.906 (3)	8.967 (2) ^d	8.963 (2)	8.971 (2)	8.978 (1)	8.993 (2)	

^a All samples were hydrated, except where indicated otherwise. ^b Second phase: 8.849 (3) Å. ^c Second phase: 8.852 (4) Å. ^d Second phase: 8.852 (2) Å. Two phases were present in these three samples, probably because at such a low silver loading (0.1 Ag/uc) the silver did not penetrate into the centers of the microcrystals, so that a cherry-type system was formed with a higher loading of silver in the outer shell than in the core. ^e Value for dehydrated NaOH-SOD taken from Luger et al.¹⁶ Dehydrated AgOH-SOD has a unit cell size of 8.786 (2) Å.

thus providing evidence for the retention of some degree of structural hydrogen bonding in the series of hydrated samples, even in the presence of bromide. A monotonic cage contraction effect with increasing bromide content is observed within the dehydrated series.

In the analogous series of hydrated silver sodalites, a slight contraction of the unit cell is observed for higher bromide concentrations (Figure 1). This can again be understood by invoking electrostatic effects due to an interaction between the halide, cations, and framework oxygens. The difference in cell dimensions between corresponding sodium and silver sodalites is small, as these cations have nearly identical radii (4-coordinate $r(\text{Na}^+) = 1.13$ Å, $r(\text{Ag}^+) = 1.14$ Å).¹² The exceptional cell expansions after introduction of silver to bromide-free Na[]-SOD may be related to differences in hydrogen bonding for the two cations, water, and framework oxygens. This effect will be discussed later in more detail.

In contrast to the bromohydrosodalites, NaBr[]-SOD, the unit cell of the hydrated bromohydroxosodalites, NaBrOH-SOD, increases monotonically as the bromide content rises. In this case the effect is spatial, the larger bromide ion requiring more room than the hydrated hydroxide ion. In basic sodalite, no essential

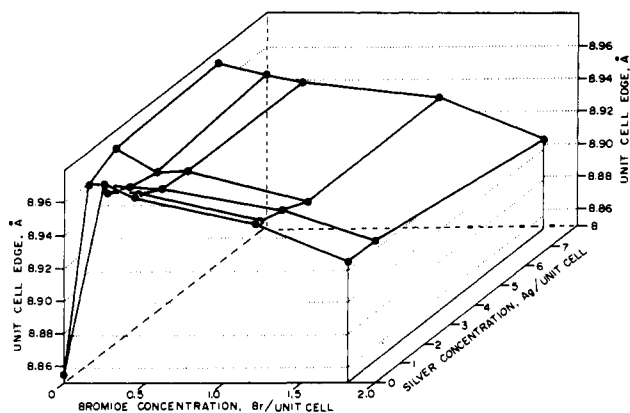


Figure 1. Unit cell size versus composition diagram for the series of hydrated sodalites of the type Na_{8-p-2n}Ag_{2n}Br_{2-p}[]_p-SOD, where $p = 0-2$, $2n = 0-8$.

H-bonding exists between framework oxygens and those of the trapped water/hydroxyl groups, and the unit cell is known to

Table V. Structural Parameters of Class B Sodalites^a

sample	ref	uc edge (Å)	∠Al-O-Si (deg)	C-X (Å)	X-X (Å)	M-M _x (Å)	M-M _i (Å)	M-O (Å)
NaOH-SOD·2H ₂ O	8	8.890	138.7	2.70	7.70	4.82	4.41	2.38
NaOH-SOD (dehyd)	16	8.7342	132.9	2.40	7.56	4.92	3.92	2.35
Na[]-SOD·8D ₂ O	15	8.8160				5.05	3.77	2.47
Na[]-SOD·8H ₂ O	14	8.848	136.2			5.08	3.76	2.51
Na[]-SOD (dehyd)	14	9.122	156.3			4.58	6.06	2.56
NaBr[]-SOD BrLI	own	8.9615	142.0	2.76	7.76	4.84	4.51	2.45
NaBr-SOD	own	8.9305	140.6	2.89	7.73	4.74	4.72	2.36
Na ₇ Ag ₁ Br[]-SOD BrLI	own	8.9581	141.1	2.83(Na) 2.39(Ag)	7.76	4.79	4.62	2.40
Ag[]-SOD	own ^b	8.9803				5.01	3.89	2.62
AgBr[]-SOD BrLI	own	8.9566	142.8	2.80	7.76	4.85	4.53	
AgBr[]-SOD BrLII	own	8.9542	143.7	2.68	7.75	4.81	4.57	2.41
AgBr[]-SOD BrLIII	own	8.9306	137.9	2.68	7.73	4.88	4.38	2.49
AgBr-SOD	own	8.9109	141.7	2.67	7.72	4.87	4.38	2.38
Ag[]I-SOD ILI	own ^b	8.9677		2.73	7.77	4.86	4.36	2.44

sample	coordinates			M	water O _x = O _y = O _z	C-OH ₂ (Å)	O ₁ -O ₂ (Å)	O-6 (Å)
	O _x	O _y	O _z					
NaOH-SOD·2H ₂ O	0.1506	0.4399	0.1397	0.1755				
NaOH-SOD (dehyd)	0.1458	0.4265	0.1370	0.1587				
Na[]-SOD·8D ₂ O	0.1455	0.4313	0.1363	0.151	0.3773	2.44	2.99	1.94
Na[]-SOD·8H ₂ O	0.1490	0.4338	0.1366	0.1504	0.3753	2.46	2.96	1.92
Na[]-SOD (dehyd)	0.1550	0.489	0.1450	0.235				
NaBr[]-SOD BrLI	0.1504	0.4470	0.1417	0.1779	0.3882	2.73	3.11	2.15
NaBr-SOD	0.1505	0.4439	0.1409	0.1867				
Na ₇ Ag ₁ Br[]-SOD BrLI	0.1506	0.4455	0.1420	0.1825(Na) 0.1537(Ag)	0.3938	2.76	3.17	2.23
Ag[]-SOD					0.1782	3.03		1.44
AgBr[]-SOD BrLI	0.1386	0.4424	0.1323	0.1805	0.3455	3.02	2.80	1.48
AgBr[]-SOD BrLII	0.1443	0.4476	0.1410	0.1730	0.3096	3.26	2.45	0.92
AgBr[]-SOD BrLIII	0.1457	0.4363	0.1379	0.1738	0.3580	2.85	2.82	1.67
AgBr-SOD	0.1456	0.4438	0.1393	0.1730				
Ag[]I-SOD ILI				0.1758	0.3367	3.04		1.35

sample	wR _p	R _p	χ ²	sample	wR _p	R _p	χ ²
NaBr[]-SOD BrLI	10.6	7.8	3.4	AgBr[]-SOD BrLII	9.8	7.3	2.1
NaBr-SOD	17.0	11.3	6.9	AgBr[]-SOD BrLIII	11.4	7.9	3.0
Na ₇ Ag ₁ Br[]-SOD BrLI	10.5	7.3	2.9	AgBr-SOD	13.5	9.9	2.9
Ag[]-SOD	13.9	10.6	4.1	Ag[]I-SOD ILI	13.8	10.7	4.1
AgBr[]-SOD BrLI	10.2	7.7	2.2				

^aStandard deviations for bond lengths are smaller than the least significant digit shown. All samples were hydrated, except where indicated otherwise. BrLI: 0.26 Br/uc; BrLII: 0.46 Br/uc; BrLIII: 1.2 Br/uc. C-X are cation to cage center distances; X-X the anion-anion separations between cages; M-M_x intercage cation separations; M-M_i intracage cation separations; M-O are cation to framework oxygen distances; C-OH₂ the cation to water oxygen distances; O₁-O₂ distances between water oxygens and framework oxygens; O-6 distances between water oxygens and the center of the six-rings. ^bData tentative for these samples due to poor refinement for the framework atoms.

contract after dehydration.^{15,16}

Rietveld Refinement. Class B sodalites can be compared to the mineral nosean.^{17,18} Nosean has the ideal composition Na₈[Al₆Si₆O₂₄](SO₄)₂·H₂O and contains ordered clusters of the types [Na₄SO₄]²⁺ and [Na₄·H₂O]⁴⁺ in a 1:1 ratio. The ordering has been ascribed to a difference in the net charge and size of these clusters. Antiphase domain boundaries arise from the ordering of clusters. Each domain belongs to the space group *P*23, a subgroup of *P*43*n*. The average space group is *P*43*n*. The cluster ordering leads to positional modulations of the framework oxygens, i.e., two well-defined framework oxygen atom positions in nosean. Superstructure reflections in sulfatic sodalites generally do not give rise to an integral multiple cell;¹⁹ their superstructures are thus incommensurate.^{17,18}

Rietveld refinements of high-resolution powder XRD data were carried out on several samples of the Na_{8-2n-p}Ag_{2n}Br_{2-p}[]_p-SOD series for *n* = 0, *p* = 0, 1, 7, 2 and *n* = 4, *p* = 0, 0.8, 1.5, 1.7, 2. The crystallographic data are given in the supplementary material. No superstructure reflections were observed in the powder patterns, indicating the absence of guest ordering. Only one average type of framework oxygen was therefore refined. Si-Al ordering in the framework was indicated by the ²⁹Si MAS NMR spectrum

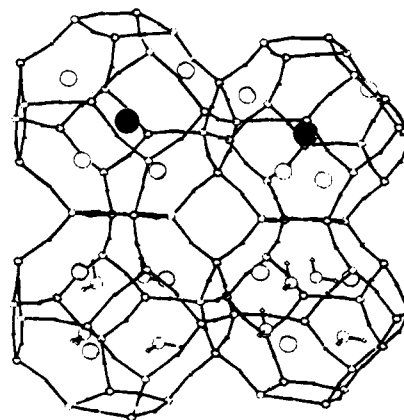


Figure 2. Sodalite cages showing the positions of anions (●), cations (○), and water molecules.

of typical silver-exchange parent materials which exhibited only one sharp peak (NaAgBrOH-SOD BrLIII, 2 Ag/uc, *a*₀ = 8.929 (2) Å, -85.3 ppm versus TMS; AgOH-SOD, *a*₀ = 8.786 (2) Å, -81.3 ppm; compared to, for example, NaOH-SOD, -84.3 ppm hydrated, -81.0 ppm dehydrated²⁰). Most samples refined well assuming an average space group *P*43*n* and a solid solution of

(15) Felsche, J.; Luger, S.; Fischer, P. *Acta Crystallogr.* 1987, C43, 809-811.

(16) Luger, S.; Felsche, J.; Fischer, P. *Acta Crystallogr.* 1987, C43, 1-3.

(17) Hassan, I.; Grundy, H. D. *Can. Mineral.* 1989, 27, 165-172.

(18) Hassan, I.; Buseck, P. R. *Am. Mineral.* 1989, 74, 394-410.

(19) Taylor, D. *Contrib. Mineral. Petrol.* 1967, 16, 172-188.

(20) Engelhardt, G.; Luger, S.; Buhl, J. C.; Felsche, J. *Zeolites* 1989, 9, 182-186.

Table VI. Effect of Cation Parameters on the Refinement of Class B Sodalites

sample	refinement ^a	wR_p	R_p	χ^2	M	M-O (Å)	M-X (Å)	M-OH ₂ (Å)
NaBr[]-SOD BrLI	Na iso	10.6	7.8	3.4	0.1779	2.445	2.762	2.73
	Na aniso	10.4	7.7	3.3	0.1770	2.455	2.748	2.71
AgBr[]-SOD BrLI	Ag iso	10.2	7.7	2.2	0.1805	2.414	2.800	2.55
	Ag aniso	10.1	7.5	2.2	0.1800	2.413	2.793	2.55
	2Ag iso	10.1	7.6	2.2	0.188	2.375	2.91	2.44
					0.171	2.472	2.65	2.70
AgBr[]-SOD BrLII	Ag iso	9.8	7.3	2.1	0.1730	2.487	2.679	2.10
	Ag aniso	9.6	7.1	2.0	0.1720	2.493	2.668	2.13
AgBr[]-SOD BrLIII	Ag iso	11.4	7.9	3.0	0.1738	2.379	2.689	
	Ag aniso	11.3	7.6	2.9	0.1736	2.380	2.686	

^aiso = thermal parameters refined isotropically. aniso = thermal parameters refined anisotropically.

cages (commensurate) with or without bromide ions (Figure 2). With the exception of one sample, all R factors were in the ranges $wR_p = 9.8$ – 13.5% , $R_p = 7.3$ – 9.9% , so that good unit cell sizes as well as the locations and separations between framework and guest atoms could be determined. Table V summarizes the results from the refinements and lists structural parameters of related sodalites from the literature.

One may expect silver to occupy more than one type of position, depending on the additional guest species present in each cage. Structural refinements were therefore carried out using one average type of silver (both isotropic and anisotropic temperature factors) or two types of silver atoms (corresponding to silver tetrahedra and silver triangles with vertices situated on the 3-fold axes near the sodalite six-rings) (Table VI). The Ag-X distance (X = Br or center of cage) obtained from the isotropic calculations turned out to be the mole fraction weighted average of the two distances obtained in the calculation where two silver atoms were allowed. The two positions were so close (within 0.26 Å) that they could not be reliably resolved by using a scan range to $100^\circ 2\theta$ with Cu K α radiation. An EXAFS analysis²¹ was also unable to distinguish between two silver sites. Even when anisotropy was invoked, the final temperature factors refined to nearly spherical symmetry. The R factors for each calculation were so similar that a choice between the three alternatives could not be made. Data corresponding to the average isotropic silver atoms are presented here.

Because of the presence of hydrogen bonding in hydrated samples, the cage dimensions and Al-O-Si angles depend strongly on the water content. For example, in Na[]-SOD, depending on the degree of dehydration, a_0 varies from 8.87 (4 H₂O/cage) to 9.11 Å (no H₂O).⁵ Any ions that interact with water have a significant effect on unit cell parameters. The effect of hydrogen bonding leads to a much larger range of Al-O-Si angles than in class A and class C sodalites:^{2,22} 133–156°. The increase in range also applies to the x , y , and z coordinates of framework oxygens which are involved in the hydrogen bonding.

In situations where water is not hydrogen-bonded (NaOH-SOD) it performs only a space-filling role. Complete dehydration results in a contraction of the cage.¹⁰ However, whenever hydrogen bonding via the water occurs, as in Na[]-SOD, the water pulls the six-ring oxygen atoms closer together (distance of framework oxygens to center of six-ring: Na[]-SOD_{hyd} < NaBr-SOD < NaBr[]-SOD BrLI < Na[]-SOD_{dehyd}); the concomitant tilting causes a cage contraction. In addition, a strong interaction between sodium ions and water oxygens draws the water molecules toward the sodium ions. The Na-O_{water} distance of 2.44–2.46 Å compared well with the literature distance²³ reported for aqueous sodium ions of 2.40–2.50 Å. With tetrahedral arrangements of cations and water (or pseudotetrahedral for three cations in four sites), the net pull is toward the center of the cage, resulting in cage contractions (distance of framework oxygen to center of cage: Na[]-SOD_{hyd} < NaBr-SOD < NaBr[]-SOD BrLI < Na[]-

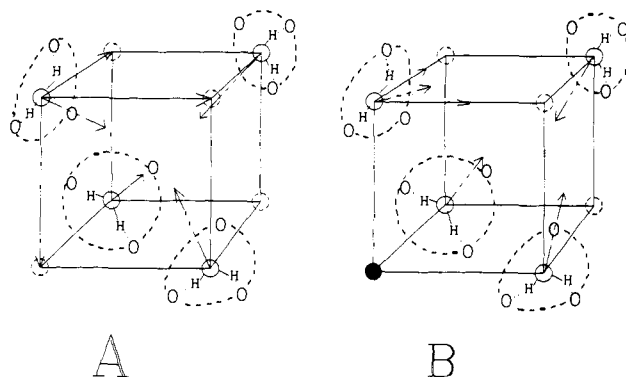


Figure 3. Proposed hydrogen-bonding effects in NaAg[]-SOD. (A) When four Na⁺ cations are present, the interaction between an O_{water} atom and adjacent cations is equal in all three directions, leading to a net force on this oxygen toward the center of the cage. The cage contracts (small unit cell). (B) When one Na⁺ cation has been replaced by Ag⁺, the interaction between an O_{water} atom and adjacent cations is not equal in all three directions. The force vectors do not point toward a common intersection. In spite of possible distortions, the net pull is not toward the center of the cage. The unit cell is therefore larger.

SOD_{dehyd}). In those instances, dehydration removes the "ties", yielding a cell expansion.¹⁰

The present study has shown that addition of a little silver to hydrated class B sodalites causes a large unit cell size increase. This effect cannot be spatial as the ionic radii of 4-coordinate Ag⁺ and Na⁺ are virtually equal. It is proposed that the expansion originates from the different hydration tendencies of Ag⁺ compared to Na⁺. For low hydration numbers, gas-phase silver ions have been shown to bind to water more strongly than sodium ions.²⁴ This behavior has been related to the tendency of silver ions to exhibit 2-fold coordination due to mixing of d_{z^2} , s , and p_z orbitals.²⁵ In the confinement of the sodalite cage, however, linear coordination with water is not possible. The refinement data show that silver ions are less strongly associated with the water molecules than the sodium ions are (longer cation-water oxygen separation: >2.8 Å, compared to literature values²³ of aqueous Ag⁺ of 2.31–2.43 Å). The water molecules are not drawn as closely to the silver ions and therefore move closer to the six-rings. While the six-ring oxygens are still bridged by water molecules through hydrogen bonding ($d(\text{O}_{\text{framework}} - \text{O}_{\text{water}}) < 3.5$ Å in all cases¹⁰), they are now not pulled strongly to the cation. In this case a less favorable orbital overlap between silver and water may lead to a lower binding energy compared to sodium, resulting in the longer cation-water separations that were observed in the silver sodalites. As soon as the first silver ion is added, it breaks the tetrahedral symmetry of the cation cluster. The net force on the water molecules which pull the framework oxygens is no longer toward the cage center, although framework distortion may still occur. The result is a drastic framework expansion even at low silver

(21) Moller, K.; Ozin, G. A.; Stein, A. Unpublished results.

(22) Stein, A. Ph.D. Thesis, University of Toronto, Toronto, Ontario, Canada 1991.

(23) Burgess, J. *Ions in Solution*; Ellis Horwood Ltd.; Chichester, England, 1988.

(24) Peterson, K. I.; Holland, P. M.; Keesee, R. G.; Lee, N.; Mark, T. D.; Castleman, A. W., Jr. *Surf. Sci.* **1981**, *106*, 136–145.

(25) Cotton, F. A.; Wilkinson, G. *Advanced Inorganic Chemistry*, 4th ed.; Wiley: New York, 1980; pp 255, 263.

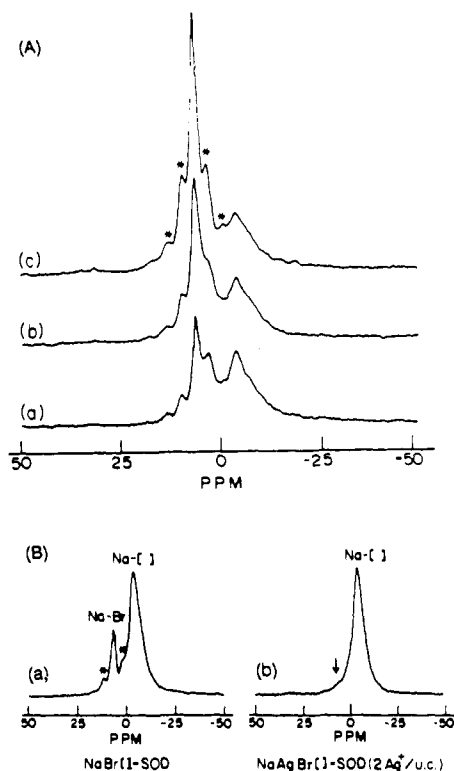


Figure 4. ^{23}Na DOR NMR spectra of (A) $\text{NaAgBr}[\]\text{-SOD}$ (BrLIII) with (a) 2 Ag/uc, (b) 1 Ag/uc, and (c) 0 Ag/uc and (B) $\text{NaAgBr}[\]\text{-SOD}$ (BrLI) with (a) 0 Ag/uc and (b) 2 Ag/uc. Asterisks denote spinning side bands.

concentrations (see Figures 1 and 3).

In the hydroxide series a small addition of silver also causes a drastic expansion of the unit cell. In hydroxosodalites, hydrogen bonding between the framework and guest constituents is not invoked, as the separation between framework oxygens and oxygens in the complex cation $(\text{Na}_4\text{OH}\cdot\text{H}_2\text{O})^{3+}$ exceeds 3.5 \AA .¹⁰ Because of the different hydration behavior for Na^+ and Ag^+ , replacement of Na^+ by Ag^+ ions may lead to rearrangement of the complex cation and change its space-filling character, resulting in the observed unit cell expansion.

Anion Distribution. Spectra obtained by mid- and far-IR, MAS NMR, and powder XRD showed single sets of peaks whose positions depended on the sample composition rather than revealing a superposition of peaks corresponding to the end members of the series ($p = 0$, $p = 2$). These results point to a 3D commensurate, compositionally disordered solid-solution model instead of one involving ordering (crystallographic superlattice), domains, or complete segregation of M_4Br and M_3 aggregates ($\text{M} = \text{Na}^+$, Ag^+). The $(2-p)\text{M}_4\text{Br}$ clusters are randomly organized in the sodalite lattice of $p\text{M}_3$ spectator cationic triangles.

Cation Distribution. In partially silver-exchanged class A sodalites, where every β -cage is filled with only one type of halide anion, silver is distributed randomly throughout the lattice.² However, for class B sodalites, both UV-visible reflectance and double rotation (DOR) ^{23}Na NMR spectroscopy provided evidence for preferential silver aggregation in halide-containing cages over anion-free cages at intermediate bromide and silver loadings. Figure 9 shows UV-visible reflectance spectra for the whole range of bromide concentrations of $\text{NaAgBr}[\]\text{-SOD}$ with 2 and 8 Ag/uc, respectively. At full silver exchange, but intermediate Br loading, the spectrum shows features associated with silver in both Br cages and $[\]$ cages (see below). In only partially silver-exchanged $\text{NaAg}[\]\text{-SOD}$, a strong absorption due to Ag^+ in the anion-free cages is observed. However, when bromide is present in partially exchanged samples, absorption features pertaining to silver in bromide cages predominate in all cases, indicating that silver accumulates preferentially in the halide-containing cages where stronger covalent bonding between Ag and X is possible.

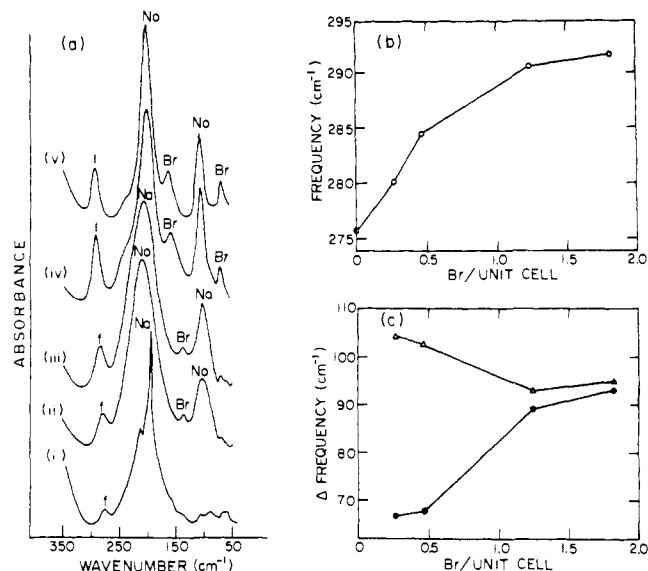


Figure 5. (a) Far-IR spectra for the series of dehydrated sodalites of the type $\text{Na}_{8-p}\text{Br}_{2-p}[\]_p\text{-SOD}$: (i) $p = 2$, (ii) $p = 1.7$, (iii) $p = 1.5$, (iv) $p = 0.8$, (v) $p = 0$. (b) Shift in the far-IR pore opening mode with Br^- loading. (c) Changes in the far-IR correlation splitting between the high-frequency and low-frequency modes of Na^+ (Δ) and Br^- (\bullet) with Br^- loading.

NMR spectroscopy (see below) was utilized to monitor the changes that occurred at specific cation sites after silver exchange. Figure 4A shows ^{23}Na DOR NMR spectra of $\text{NaAgBr}[\]\text{-SOD}$ (BrLIII) (Table III) containing 2 and 1 Ag/uc and their silver-free parent sodalite. In the parent material, two sodium resonances are observed at 5.3 ppm (associated with Br cages) and -4.6 ppm (associated with $[\]$ cages) versus a dilute aqueous NaCl solution. For silver-exchanged samples, the intensity of the resonance corresponding to the Br cages is progressively reduced with increasing silver content. At the same time the second resonance remains at nearly constant intensity. In samples with lower bromide loading (BrLI), the high-frequency resonance disappeared almost completely after two Na^+ ions per unit cell had been replaced by silver (Figure 4B). The loss in intensity indicates that the sodium concentration is reduced in those cages containing bromide before the ones containing no anion. Similar observations were made in NaAgBrOH-SODs . Extended Hückel molecular orbital calculations have shown that in NaAgX-SOD a bonding MO interaction exists between Ag orbitals and X orbitals. On the other hand, in $\text{NaAg}[\]\text{-SOD}$ no overlap of bonding orbitals of Ag with any other species develops (water not considered). Because of the strength of the silver-bromide bond, there is a clear preference for the silver to exchange sodium cations in bromide cages, rather than to exchange sodium in empty or hydroxide cages. Domains of higher silver concentration were too small ($50\text{--}200 \text{ \AA}$) to be resolved by powder X-ray diffraction, as they are controlled by the solid-solution model proposed for the anions (above).

Cluster Interactions: Vibrational Coupling

A comparison of the trend in atomic separations (Table V) with the corresponding far-IR spectra reveals a dependence of the vibrational coupling on the bromide content of these samples. The far-IR spectra for samples with varying bromide content (Figure 5a) show the effect of dropping the population of Na_4Br clusters from two to zero per unit cell of sodalite. The smoothness of this transformation is demonstrated by the monotonic low-frequency shift of the pore opening framework mode with decreasing halide concentration (Figure 5b). The splitting of the Br^- anion correlation couplet²⁶ seen at 161 and 68 cm^{-1} decreases as the average separation between bromides becomes greater (larger p) (Figure

(26) Godber, J.; Ozin, G. A. *J. Phys. Chem.* 1988, 92, 2841–2849, 4980–4987.

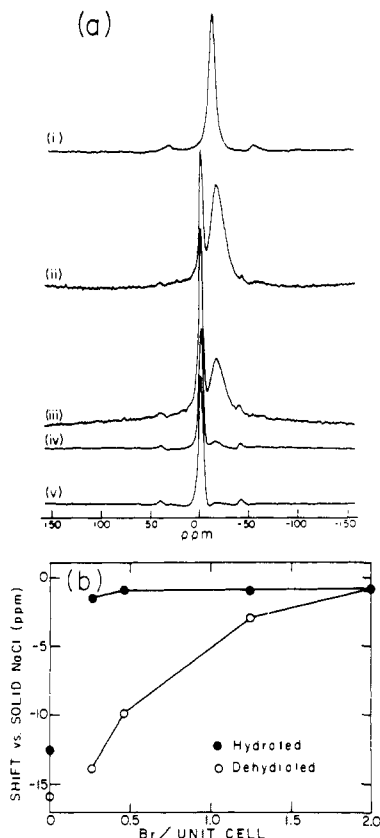


Figure 6. (a) ^{23}Na MAS NMR spectra of hydrated $\text{Na}_{8-p}\text{Br}_{2-p}[\]_p\text{-SOD}$: (i) $p = 2$, (ii) $p = 1.7$, (iii) $p = 1.5$, (iv) $p = 0.8$, (v) $p = 0$. (b) Dependence of the ^{23}Na MAS NMR shifts of the Na_4Br resonance relative to solid NaCl on the Br^- concentration for hydrated (●) and dehydrated (○) samples.

5c). Its intensity subsequently goes to zero. However, the Na^+ cation correlation couplet observed at 200 cm^{-1} (E) and 105 cm^{-1} (A_1) remains, and each band broadens, due to an inhomogeneous distribution of $\text{Na}_4\text{Br}/\text{Na}_3$. Even at one Br^- approximately every fourth cavity ($p = 1.54$), the collective vibrational coupling between Na_4Br clusters has been severely suppressed. The absence of the correlation splitting in anion-free $\text{Na}[\]\text{-SOD}^{26}$ demonstrates the requirement of Br^- for effective coupling between the Na^+ ions of adjacent β -cages.

The correlation splitting between the sodium translational modes decreases slightly as bromide is added to the sodalite. If the coupling depended solely on the separation between Na^+ ions in adjacent cages, one would expect the opposite trend since the $\text{Na}-\text{Na}$ separation between adjacent cages was found to decrease at higher Br^- loadings. However, the $\text{Na}-\text{X}$ separation increases at the same time. This provides further evidence that the anion plays a significant mediation role in the coupling between Na^+ ions. Since nonbasic hydrosodalite, containing only cationic triangles, exhibits no correlation coupling, it is likely that at dilute bromide concentrations the Na^+ coupling occurs predominantly between cages containing sodium tetrahedra. The overall effect is therefore complicated by the extent of connectivity between MBr_4 clusters throughout the lattice. Similar, but less pronounced, effects can be discerned in the far-IR spectra of the corresponding fully Ag^+ -exchanged $\text{Ag}_{8-p}\text{Br}_{2-p}[\]_p\text{-SOD}$. The $\text{Ag}-\text{X}$ distance decreases at higher Br^- loadings. One might expect an increase in $\text{Ag}-\text{Ag}$ correlation coupling. Unfortunately the correlation couplet A_1 type partner of the E type silver translational mode at 91 cm^{-1} was not observed in the experimental range down to 50 cm^{-1} , and the above idea could not be tested with the silver samples.

Cluster Interactions: Electronic Coupling

Solid-State NMR Spectroscopy. Evidence for collective electronic interactions stems from both the ^{23}Na NMR spectra and

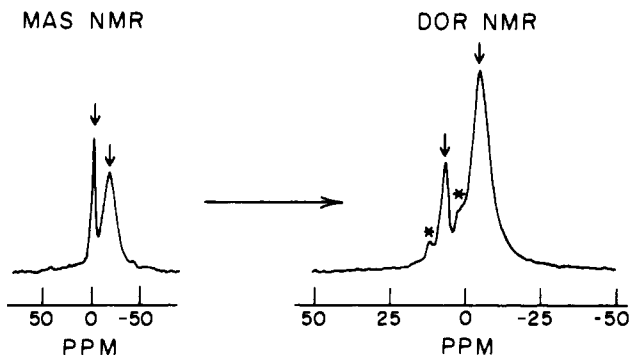


Figure 7. ^{23}Na NMR spectra of $\text{NaBr}[\]\text{-SOD}$ (BrLI) showing the similarity between MAS and DOR results for this type of sample. Asterisks denote spinning side bands.

UV-visible absorption spectra. ^{23}Na MAS NMR spectra of hydrated class B sodium sodalites show two components, a sharp band (full width at half-height (FWHH): $310\text{--}380\text{ Hz}$) ca. 1 ppm upfield from solid NaCl and a broad band (FWHH: $1200\text{--}1350\text{ Hz}$) ca. 17 ppm upfield from the reference sample (Figure 6). The relative intensity of the sharp to the broad absorption increases as more bromide is added. In a sample which contains essentially all Br cages, the band at -17 ppm is virtually absent. (A small remnant is an indicator for some defects: hydroxide- or water-containing cages. It may be used as a gauge to estimate the concentration of such defects.) One may therefore assign the broad resonance to sodium in anion-free cages. A linear correlation between the ratios of sodium in Br and $[\]$ cages obtained from a chemical analysis and the ratios of the two peak areas confirms the assignment. Rapid chemical exchange between the two cation sites, which has been observed in other hydrated zeolite samples,²⁷ did not occur as it would have produced a single Na^+ line. Double rotation ^{23}Na MAS NMR spectra^{28a} show the same two features, indicating that quadrupolar effects can be neglected in the qualitative interpretation of these spectra (Figure 7).

In dehydrated samples only one resonance is observed which increases in intensity and shifts downfield with higher Br^- loading. This peak is assigned to the ^{23}Na resonance in cages containing Na_4Br . The absence of an observable peak corresponding to Na_3 cationic triangles indicates that intensity loss has occurred through line broadening as a result of greater localization of cations in the cation sites of the $[\]$ cages²⁹ and of locating the bare Na^+ ions in less symmetric environments than hydrated sodium ions.³⁰ This greatly increases the quadrupolar interactions.³¹ (In a hydrated sample the electric field gradient produced by induced dipoles at the sites of the oxygen ions³² is averaged by the motion of water molecules.³³) Chemical exchange of Na^+ between cages is not expected at room temperature for dehydrated sodalites.²⁷ In the dehydrated samples the shift of the Na_4Br resonance with increasing Br^- loading is attributed mainly to deshielding of sodium due to electron withdrawal by the relatively electronegative bromide ion, thereby providing evidence for electronic coupling between Na_4Br clusters. Any effects involving charge transfer by framework oxygens must be negligible as they would result

(27) Kundla, E.; Samoson, A.; Lippmaa, E. *Chem. Phys. Lett.* **1981**, *83*, 229-232.

(28) (a) Jelinek, R.; Chmelka, B.; Stein, A.; Ozin, G. A. *J. Phys. Chem.*, in press. (b) Jelinek, R.; Stein, A.; Ozin, G. A. *J. Am. Chem. Soc.*, submitted for publication.

(29) Welsh, L. B.; Lambert, S. L. In *Characterization and Catalyst Development*; Bradley, S. A., Gattuso, M. J., Bertolacini, R. J., Eds.; ACS Symposium Series 411; American Chemical Society: Washington, D.C., 1989; pp 262-272.

(30) Engelhardt, G.; Michel, D. *High Resolution Solid-State NMR of Silicates and Zeolites*; John Wiley & Sons: New York, 1987.

(31) Tjink, G. A. H.; Janssen, R.; Veeman, W. S. *J. Am. Chem. Soc.* **1987**, *109*, 7301-7304.

(32) Lechert, H. In *Molecular Sieves*; Meier, W. M., Uytterhoeven, J. B., ACS Advances in Chemistry Series 121; American Chemical Society: Washington, D.C., 1974; pp 74-86.

(33) Klinowski, J. *Prog. Nucl. Magn. Reson. Spectrosc.* **1984**, *16*, 237-309.

Table VII. ^{23}Na Resonances of Class B Sodium Sodalites

sample	Br/uc	treatment	uc Size (Å)	MAS shift ^a (ppm)	$R(\text{pk})^b$	$R(\text{an})^b$
Na[]-SOD BrL0	0.00	hydrated	8.849	-12.8		
Na[]-SOD BrL0	0.00	hydrated	8.854	-12.6	0.00	0.00
NaBr[]-SOD BrLI	0.26	hydrated	8.972	-1.5, -17.6	0.53	0.24
NaBr[]-SOD BrLII	0.46	hydrated	8.964	-0.9, -17.1	1.42	0.52
NaBr[]-SOD BrLIII	1.18	hydrated	8.948	-1.0, -16.1	6.00	2.43
NaBr[]-SOD BrLA	1.39	hydrated	8.946	-1.2, -17.1	13.3	4.75
NaBr[]-SOD BrLB	1.63	hydrated	8.899	-1.4	15.6	6.94
NaBr-SOD BrLF	1.82	hydrated	8.927	-0.8, -17.5	15.6	7.76
Na[]-SOD BrL0	0.00	dehydrated	9.092	-15.9		
NaBr[]-SOD BrLI	0.26	dehydrated	9.053	-13.9		
NaBr[]-SOD BrLII	0.46	dehydrated	9.019	-9.9		
NaBr[]-SOD BrLIII	1.18	dehydrated	8.959	-2.9		
NaBr-SOD BrLF	1.82	dehydrated	8.958	-0.8		
NaOH-SOD BrL0	0.00	hydrated	8.902	-13.8 (-14.0)	0.00	0.00
NaBrOH-SOD BrLI	0.29	hydrated	8.916	-0.8, -16.6	1.08	0.21
NaBrOH-SOD BrLII	0.51	hydrated	8.920	-0.8, -16.4	1.82	0.44
NaBrOH-SOD BrLIII	1.29	hydrated	8.933	-0.9, -15.8		2.32
NaBrOH-SOD BrLA	1.44	hydrated	8.934	-1.0, -17.2	14.8	2.98
NaBr-SOD BrLF	1.82	hydrated	8.927	-0.8, -17.5	15.6	7.76

^a MAS shifts are given in ppm versus solid NaCl. ^b $R(\text{pk})$ refers to the intensity ratios of the high-frequency to the low-frequency peak. $R(\text{an})$ refers to the analytically determined ratio of Na^+ in Br cages to Na^+ in [] or OH cages. A plot of $R(\text{an})$ versus $R(\text{pk})$ of the first five NaBr[]-SOD samples results in a straight line with a correlation coefficient of 0.998. For the NaBrOH-SOD samples the correlation coefficient is 0.9996 for all values excluding the last sample which has a great uncertainty in the area of the low frequency peak. The peak positions of the resonances for the dehydrated NaBrOH-SOD samples were not measured because of strong peak broadening and asymmetry.

in the opposite trend: as the bromide concentration increases, the unit cell size and T-O-T angles both decrease,³⁴ allowing more charge density to relocate from the sodalite-cage lattice six-ring oxygen to $\text{Na}^+(3s)$, especially as the Na-O separation is reduced at the same time. As in the case of the unit cell sizes, one has to consider the role of imbibed water to interpret the ^{23}Na chemical shifts of the hydrated bromohydrosodalites. In these samples, as the Br^- loading increases, the water content correspondingly decreases. The structural water in the cages containing cationic triangles has the effect of deshielding the sodium cations in bromide-containing β -cages. This occurs presumably by withdrawing charge density from the framework oxygens via hydrogen bonding. Further insight into these systems has recently been provided by Ag^+ loading dependent ^{23}Na DOR NMR and ^{81}Br , ^{35}Cl MAS NMR studies.^{28a,b}

^{23}Na MAS NMR spectra for samples containing both OH^- and Br^- anions, (i.e., the precursors to the above samples before Soxhlet extraction) are shown in Figure 8. They are all similar in appearance to spectra for samples without OH^- . Small differences in chemical shift can be related to different unit cell sizes for the two materials, with an upfield shift for larger unit cell sizes (Table VII). In these samples some NaOH may have been removed during the washing process, possibly resulting in a mixture of OH and [] cages.

Optical Spectroscopy. Optical reflectance data for $\text{Na}_{8-2n}\text{Ag}_{2n}\text{Br}_{2-p}[\]_p\text{-SOD}$, where $p = 0-2$ and $2n = 0-8$, are shown for the hydrated samples at room temperature in Figure 9. The series $p = 2$, $2n = 0-8$ serves as a pivotal control group to pinpoint those absorptions associated with $m = 0-3 \text{ Na}_{3-m}\text{Ag}_m$ ionic triangles, which all fall at 220-240 and 300 nm (Figure 9A). The absorption in the silver-free Na[]-SOD occurs at lower energy (240 nm) than in NaBr-SOD. Extended Hückel molecular orbital (EHMO) calculations indicate that this is due to the stabilization of the {Si 3s, 3p, Na 3s} levels in Na[]-SOD compared to a sodium halosodalite (Figure 10). The framework O 2p levels fall in the same energy range, whether or not the halide is present.

When silver is introduced into the anion-free sodalite, an absorption band due to the {Ag 5s, Na 3s, Si 3s, 3p} \leftarrow {Ag 4d} transition and/or the {Ag 5s, Na 3s, Si 3s, 3p} \leftarrow {Ag 5p, 4d} transition appears in the UV region. At low silver ion loading, the corresponding filled molecular orbitals (MO) are split, and structure can be observed in the optical spectrum. At higher concentrations of silver the splitting disappears as the individual

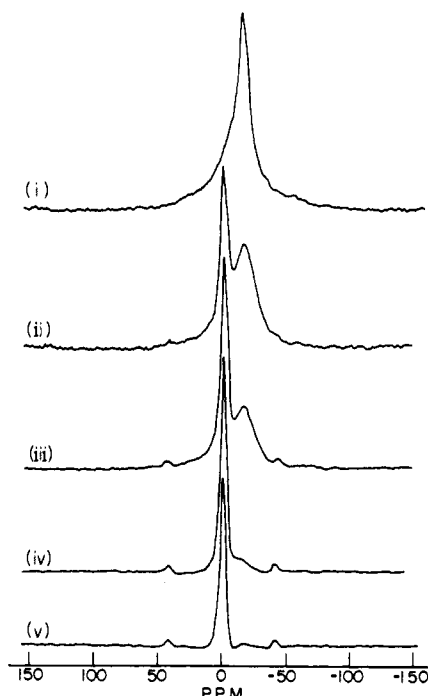


Figure 8. ^{23}Na MAS NMR spectra of hydrated $\text{Na}_8\text{Br}_{2-p}\text{OH}_p\text{-SOD}$: (i) $p = 2$, (ii) $p = 1.7$, (iii) $p = 1.5$, (iv) $p = 0.8$, (v) $p = 0$. Note the similarity with the spectra of the Soxhlet-extracted products of these samples shown in Figure 6.

MOs appear to form a valence band. At full silver exchange another absorption band is observed at ca. 305 nm. This is assigned to the {Ag 5s, 5p} \leftarrow {Ag 4d} transition, as the {Ag 5s, 5p} levels have now split away from the {Si 3s, 3p} band. In contrast to the other electronic transitions mentioned here, this transition occurs purely within cluster atoms and does not involve the framework.

Now let us consider the effects of including increasing loadings of bromide in the sodalite cages. For one Br^- in every eighth sodalite cage, the line widths of the $\text{Na}_{4-n}\text{Ag}_n\text{Br}$ cluster UV optical excitations are so narrow compared to the parent case of one Br^- per cavity (Figure 9B), that individual components for $n = 0, 0.05, 0.5, 1, 4$ can be resolved around 230, 248, 250/265, and 255/270/320 nm, respectively. When these data are compared with those of class A quantum supralattices,^{1,2} one realizes that all of

(34) Weller, M. T.; Wong, G. *J. Chem. Soc., Chem. Commun.* 1988, 1103-1104.

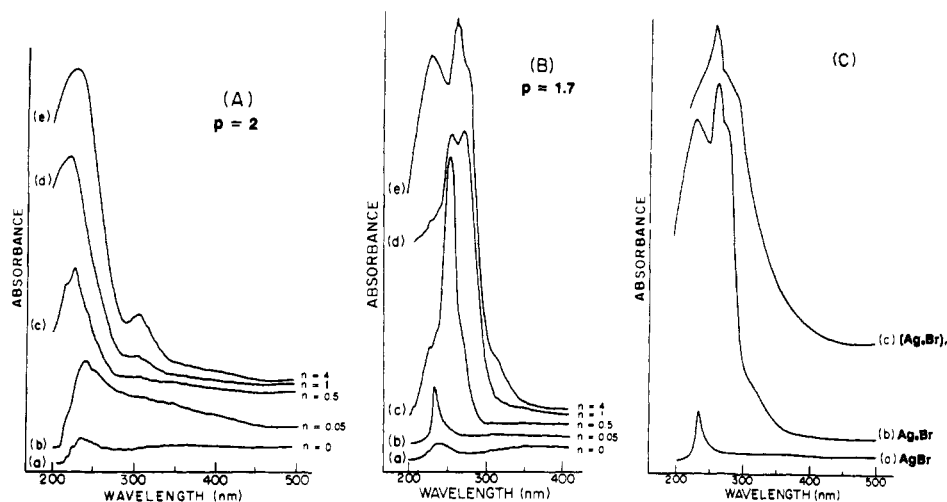


Figure 9. Optical reflectance data for some members of the hydrated sodalite series $\text{Na}_{8-2n-p}\text{Ag}_{2n}\text{Br}_{2-p}[\cdot]_p\text{-SOD}$: (A) $p = 2$; (B) $p = 1.7$ (a) $n = 0$, (b) $n = 0.05$, (c) $n = 0.5$, (d) $n = 1$, (e) $n = 4$. (C) Progression of the UV-visible spectra from the sodalite-encapsulated "isolated" AgBr molecule to the "isolated" Ag_4Br cluster and to the extended $(\text{Ag}_4\text{Br})_n$ quantum supralattice.

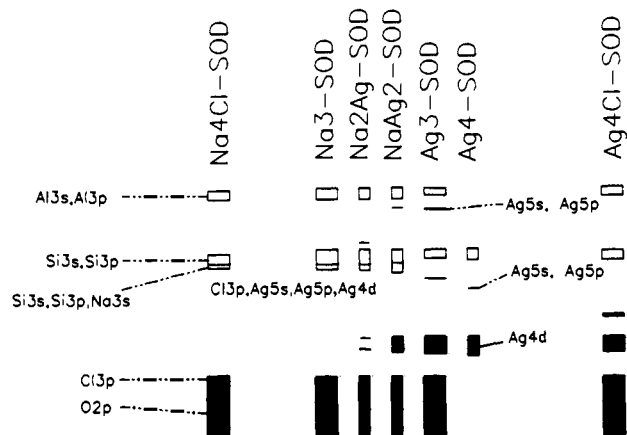


Figure 10. Sodalite band diagrams for one cluster of the type indicated, inside a single sodalite cage.

the resolved components of the class B supralattices are contained within the spectral envelope of the former. The absorption bands can be assigned by assuming a superposition of contributions from M_3^{3+} and M_4X^{3+} containing cages. For example, in the sodalite containing isolated $\text{Ag}_4\text{Br}^{3+}$ clusters (Figure 9B or C), the absorptions at ca. 230 and 320 nm can be assigned to the $\{\text{Si } 3s, 3p\} \leftarrow \{\text{Ag } 4d\}$ and $\{\text{Ag } 5s, 5p\} \leftarrow \{\text{Ag } 4d\}$ transitions, respectively, for Ag_3^{3+} cages, and those at ca. 255 and 270 nm to the $\{\text{Ag } 5s, \text{Si } 3s, 3p\} \leftarrow \{\text{Ag } 4d\}$ and $\{\text{Ag } 5s, \text{Si } 3s, 3p\} \leftarrow \{\text{Br } 4p, \text{Ag } 5s, 5p, 4d\}$ transitions, respectively, for $\text{Ag}_4\text{Br}^{3+}$ cages. These assignments are consistent with all spectra shown in Figure 9, as well as in the iodide equivalents (replacing Br 4p by I 5p) shown in Figure 11.

At low silver and bromide loadings, the very sharp UV absorption spectrum resembles that of an isolated gas-phase silver bromide monomer ($\{\text{Ag } 5s\} \leftarrow \{\text{Br } 4p, \text{Ag } 4d\}$, Figure 9Bb). It is notable that the Ag-Br bond length in $\text{NaAgBr}[\cdot]\text{-SOD}$ (BrLI, 1 Ag/uc) has the same value as that of a gas-phase AgBr molecule (2.39 Å)³⁵ and is much shorter than the Ag-Br distances in completely silver-exchanged samples.²

The reader should note that one cannot truly speak of an "isolated molecule". The observed electronic transitions do not occur completely within the molecule, but also involve the lattice. Orbital overlap of the silver cation 5s and 5p orbitals with the halide anion, sodium cations, as well as framework atoms is significant (ca. 8–28%). A more accurate term would be "a defect AgBr molecule in the $\text{Na}[\cdot]\text{-SOD}$ lattice". In fact, one cannot even speak of $\text{Ag}_4\text{Br}^{3+}$ as an "isolated cluster". Here, too, the

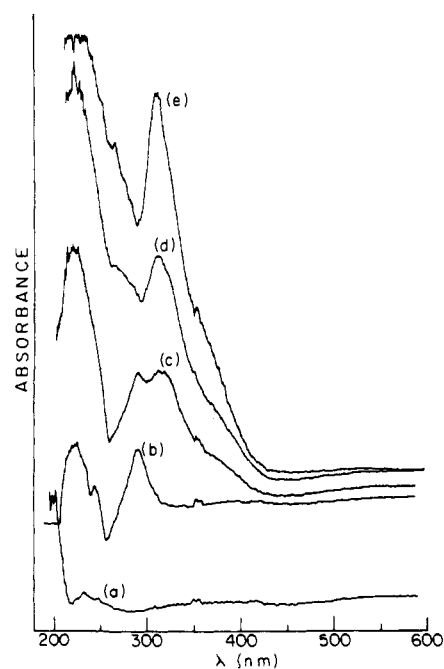


Figure 11. Optical reflectance data of hydrated sodalites of the type $\text{NaAgI}[\cdot]\text{-SOD}$ (L1), with various silver loadings: (a) 0 Ag/uc, (b) 1 Ag/uc, (c) 2 Ag/uc, (d) 4 Ag/uc, (e) 8 Ag/uc.

framework is involved in the electronic transitions, and significant overlap exists between the Ag^+ and framework constituents. Host matrix effects must therefore be considered.

The line broadening and red shift of the band edge observed when either the silver or the bromide concentration is increased indicate electronic coupling between $\text{Na}_{4-n}\text{Ag}_n\text{Br}$ clusters (Figure 9C). The absorption edge extends even further into the red for bulk AgBr.² Whereas sodium does not appear to contribute much to the coupling (the absorption bands are sharpest at high sodium concentrations), both bromide and silver must be mediating the communication between clusters. The Ag-Br and Ag-Ag separations (within each cage) change most drastically between $p = 1.7$ and $p = 1.5$. However, the most significant broadening of absorption bands in the optical spectra occurs only after the $p = 0.8$ loading level. This is an indication that the major mechanism leading to band broadening is not an increase in orbital overlap of the ions within a cage, but rather greater communication between clusters in adjacent cages as the number of bromide centers rises and their separation decreases. Broadening due to phonon coupling is an additional factor. For example, upon cooling AgBr-SOD to 27 K, three major components could be resolved

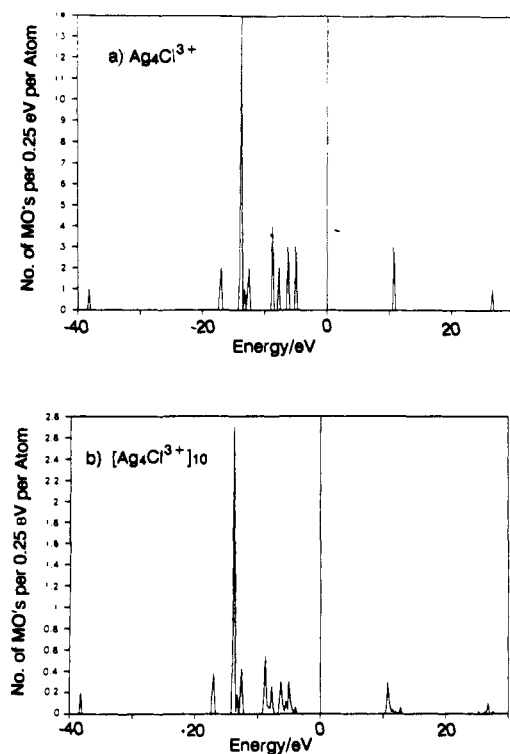


Figure 12. Density of states diagrams for (a) $\text{Ag}_4\text{Cl}^{3+}$ and (b) $[\text{Ag}_4\text{Cl}^{3+}]_{10}$. The graphs show the number of molecular orbitals per atom within 0.25 eV ranges.

completely and further components partially.

EHMO Calculations—Development of Bands. The density of states diagrams for one and ten Ag_4Cl clusters (in which the sodalite framework was not included) show the origin of band broadening as clusters couple (Figure 12). Even at the low aggregation number of ten clusters the density of states increases. By extrapolation, continuous band formation becomes possible at approximately Avogadro's number of clusters. Nevertheless, a simple increase in the density of states does not imply band formation. For that to happen, the orbitals must overlap significantly. Overlap values are proportional to the interaction between atoms.³⁶ An EHMO calculation³⁷ revealed that, at a separation of 4–5 Å between silver atoms within a cluster and between clusters, the overlap is up to 19 and 13%, respectively. Because of the large separation between clusters, the bands formed by the quantum supralattice are expected to be narrow. However, k -space band calculations would be required to probe the band width.

The effect of the number of clusters, n , on the frontier orbital levels was studied for $[\text{Ag}_3^{3+}]_n$ clusters arranged in a space-filling cubic arrangement, as they would be in a cube of nine sodalite cages (Figure 13). Even though the absolute energies obtained with and without charge iterations differed greatly, the general trend observed was the same. For aggregations of $[\text{Ag}_3^{3+}]_n$ clusters, the HOMO–LUMO gap remained nearly constant as n increased. This is in contrast to $[\text{Ag}_4\text{Cl}^{3+}]_n$ clusters, for which the gap was reduced for larger n .²

Class B sodalites contain mixtures of cages with different guest clusters. Figure 14 shows the trend in frontier orbital energies going from $[\text{Ag}_4\text{Cl}]_9$ to $[\text{Ag}_4\text{Cl}]_8[\text{Ag}_3]$, $[\text{Ag}_4\text{Cl}][\text{Ag}_3]_8$, and finally $[\text{Ag}_3]_9$ cluster aggregates. By coincidence, the energy gap in the end members is similar (374 and 395 nm for $[\text{Ag}_4\text{Cl}]_9$ and $[\text{Ag}_3]_9$, respectively). The LUMOs are composed of Ag 5s (some Ag 5p) and the HOMOs of Cl 3p, Ag 4d, Ag 5s, or only Ag 4d of their

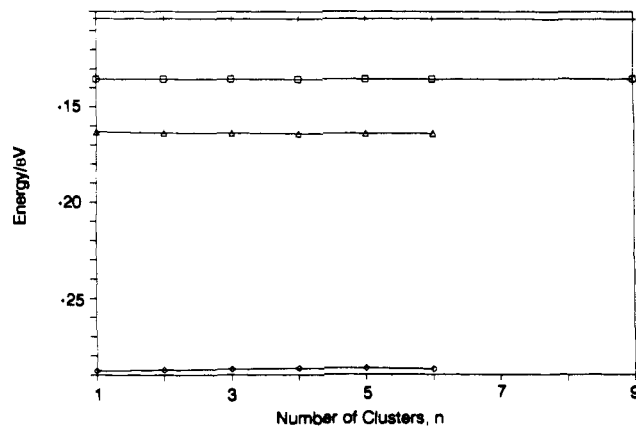


Figure 13. Effect of $[\text{Ag}_3^{3+}]_n$ cluster aggregation on the frontier orbital energies: +, LUMO (no charge iterations (CI)); □, HOMO (no CI); Δ, LUMO (CI); ◇, HOMO (CI).

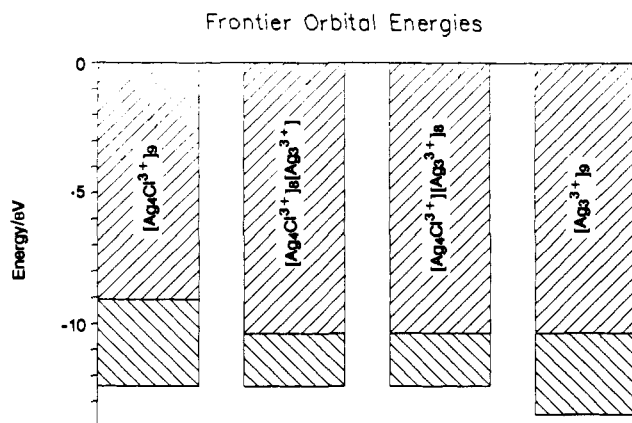


Figure 14. Effect of the Cl:[] ratio of $\text{Ag}_4\text{Cl}^{3+}$ and Ag_3^{3+} cluster aggregates on the frontier orbital energies. The horizontal lines indicate the energies of the HOMO (lower) and LUMO (upper) levels. Nine clusters were organized in a body-centered cubic arrangement for these EHMO calculations.

respective clusters. It is noteworthy that as soon as one different cluster is added as an "impurity" the gap becomes narrower and remains nearly unchanged with the relative ratio of the two types of clusters. The main reason for the constant gap is the fact that the HOMO level always is associated with an $\text{Ag}_4\text{Cl}^{3+}$ cluster and the LUMO with an Ag_3^{3+} cluster. Both of these orbital levels are only weakly dependent on the cluster size. The frontier levels of these clusters are only slightly perturbed by their neighbors. Atomic charge calculations showed that the silver atoms in Ag_3^{3+} clusters retain their full charge (+1) while in $\text{Ag}_4\text{Cl}^{3+}$ clusters the charge is alleviated by the Cl atoms (+0.46). This implies that the two types of cluster do not form mixed bands (one would otherwise expect some alteration of the charge on Ag_3^{3+} clusters) and that at low "defect" concentrations the "defect" clusters may indeed be considered isolated. On the basis of similar types of calculations for the class A sodalites,² we do not expect the inclusion of the sodalite framework to significantly affect the trends and conclusions presented above.

Conclusions

By varying the silver and halide loading of class B sodalites it is possible to create β -cage-encapsulated guests covering the range from an isolated AgX molecule to an isolated Ag_4X^{3+} cluster and an extended $(\text{Ag}_4\text{X}^{3+})_n$ cluster lattice ("expanded semiconductor"). The term "isolated" in this context means isolated from other species of the same type. The justification for using the term AgX molecule lies in the fact that the halide appears to be more closely associated with the silver ion than the sodium cations (bond lengths). In the case of the isolated molecule and cluster, the electronic states are localized. Formation of an extended cluster lattice leads to cluster interaction via vibrational and electronic

(36) Calzaferri, G.; Forss, L. *Helv. Chim. Acta* 1987, 70, 465–479.

(37) Calzaferri, G.; Forss, L.; Hugentobler, T.; Kamber, I. *ICONC* and *INPUTC*, Fortran software for extended Hückel molecular orbital calculations, Institute for Inorganic and Physical Chemistry, University of Berne, Freiestrasse 3, CH-3009 Berne, Switzerland, 1989.

coupling and possibly to delocalization. The concentration and identity of cations and anions control the extent of coupling, as shown by far-IR, ^{23}Na MAS NMR, and UV-visible spectroscopy. Results from optical spectroscopy and extended Hückel molecular orbital calculations hinted at the evolution of narrow bands. Very recent studies of the Ag^+ loading dependent ^{23}Na quadrupole coupling constants (DOR NMR) and ^{81}Br , ^{35}Cl chemical shifts (MAS NMR) in class A and class B sodium, silver halosodalites provide convincing evidence for collective electronic interactions between $\text{Na}_{4-n}\text{Ag}_n\text{X}$ clusters in the sodalite lattice.^{28a,b}

Acknowledgment. We acknowledge the Natural Science and Engineering Research Council (NSERC) of Canada's Operating

and Strategic Grants Programmes, Alcan Canada and Optical Recording Corporation, Toronto (G.A.O.), as well as the Office of Naval Research and QUEST (G.D.S.) for generous financial support of this work. A.S. thanks NSERC for a 1967 Science and Engineering Postgraduate Scholarship. We thank Raz Jelinek, Peter M. Macdonald, Michele Meszaros, Bill Harrison, and Nancy Keder for valuable technical assistance and discussions.

Supplementary Material Available: Tables of crystallographic characterization data for NaBr-SOD, $\text{Na}_{7.6}\text{Ag}_{0.3}\text{Br-SOD}$, $\text{Na}_{5.3}\text{Ag}_{2.4}\text{Br-SOD}$, AgBr-SOD, AgCl-SOD, and AgI-SOD (6 pages). Ordering information is given on any current masthead page.

Structure and Properties of Molybdenum(IV,V) Arenethiolates with a Neighboring Amide Group. Significant Contribution of $\text{NH}\cdots\text{S}$ Hydrogen Bond to the Positive Shift of Redox Potential of $\text{Mo(V)}/\text{Mo(IV)}$

Norikazu Ueyama, Taka-aki Okamura, and Akira Nakamura*

Contribution from the Department of Macromolecular Science, Faculty of Science, Osaka University, Toyonaka, Osaka 560, Japan. Received February 24, 1992

Abstract: Monooxomolybdenum(V) and monooxomolybdenum(IV) complexes with *o*-(acylamino)benzenethiolate, $(\text{NEt}_4)[\text{Mo}^{\text{V}}\text{O}(\text{S-}o\text{-RCONHC}_6\text{H}_4)_4]$ ($\text{R} = \text{CH}_3, t\text{-Bu}, \text{CF}_3$), $(\text{NEt}_4)_2[\text{Mo}^{\text{IV}}\text{O}(\text{S-}o\text{-RCONHC}_6\text{H}_4)_4]$, were synthesized and characterized by visible, ESR, ^1H NMR, and Raman spectroscopies, and electrochemical analysis. $(\text{PPh}_4)[\text{Mo}^{\text{V}}\text{O}(\text{S-}o\text{-CH}_3\text{CONHC}_6\text{H}_4)_4]\cdot\text{CH}_3\text{CN}$ crystallizes in the space group $P2_1/n$ with $a = 20.95$ (2) Å, $b = 12.509$ (2) Å, $c = 22.383$ (5) Å, $\beta = 91.8$ (1)°, $V = 5864$ (8) Å³, $Z = 4$, and $d_{\text{calcd}} = 1.311$ g cm⁻³. $(\text{PPh}_4)_2[\text{Mo}^{\text{IV}}\text{O}(\text{S-}o\text{-CH}_3\text{CONHC}_6\text{H}_4)_4]$ crystallizes in the space group $P2_1$ with $a = 14.636$ (3) Å, $b = 13.457$ (3) Å, $c = 19.341$ (2) Å, $\beta = 110.08$ (1)°, $V = 3578$ (1) Å³, $Z = 2$, and $d_{\text{calcd}} = 1.351$ g cm⁻³. Both complexes have a distorted square-pyramidal structure with an axial $\text{Mo}=\text{O}$ and two distinct kinds of Mo-S bonds. All four acylamino groups of both complexes are located at the $\text{Mo}=\text{O}$ side even in spite of the steric neighboring congestion which is similar to the reported structure of $(\text{NEt}_4)[\text{Mo}^{\text{V}}\text{O}(\text{SC}_6\text{H}_5)_4]$. All four NH groups are involved in intraligand $\text{NH}\cdots\text{S}$ hydrogen bonds with which contribute to the positive shift of $\text{Mo(V)}/\text{Mo(IV)}$ redox potential in acetonitrile. Preliminary EHMO calculations also support the $\text{NH}\cdots\text{S}$ hydrogen bonds.

Introduction

Monooxomolybdenum(V) and monooxomolybdenum(IV) complexes having thiolate ligands are of interest as model complexes for resting or reduced species of the active site of biologically important molybdooxidases. The very rapid and rapid signals appeared on the reduction of the enzymes have been considered to be dioxomolybdenum(V) species. However, a synthetic model complex $[\text{Mo}^{\text{V}}\text{O}_2\text{L}]^-$ ($\text{LH}_2 = N,N'$ -dimethyl- N,N' -bis(2-mercaptophenyl)-1,2-diaminoethane), has been considered to convert to the monooxomolybdenum(V) species in the presence of protons.¹ Crystallographic and spectroscopic analyses of various monooxomolybdenum(V) complexes containing ligand sets, e.g., S_4 , S_2N_2 , S_2O_2 , and N_3S_2 , have been reported.²⁻¹⁵ For example,

arenethiolate complexes, $[\text{Mo}^{\text{V}}\text{O}(\text{SPh})_4]^{-3}$ and $[\text{Mo}^{\text{V}}\text{O}(\text{bdt})_2]^-$ ($\text{bdt} = 1,2\text{-benzenedithiolato}$),¹⁶ and alkanedithiolate complexes, $[\text{Mo}^{\text{V}}\text{O}(\text{SCH}_2\text{CH}_2\text{S})_2]^-$,⁹ are known to have a square-pyramidal geometry. The ESR parameters in $[\text{MoOCl}_{4-x}(\text{SPh})_x]^-$ ($x = 0-4$) have been shown to be related to the number of thiolate ligands and the covalency of the Mo-S bonds.¹⁷ Nonpyramidal mono-

(1) Wilson, G. L.; Greenwood, R. J.; Pilbrow, J. R.; Spence, J. T.; Wedd, A. G. *J. Am. Chem. Soc.* 1991, 113, 6803.

(2) Yamanouchi, K.; Enemark, J. H. *Inorg. Chem.* 1979, 18, 1626.

(3) Boyd, I. W.; Dance, I. G.; Murray, K. S.; Wedd, A. G. *Aust. J. Chem.* 1978, 31, 279.

(4) Bradbury, J. R.; Mackay, M. F.; Wedd, A. G. *Aust. J. Chem.* 1978, 31, 2423.

(5) Taylor, R. D.; Street, J. P.; Minelli, M.; Spence, J. T. *Inorg. Chem.* 1978, 17, 3207.

(6) Scullane, M. I.; Taylor, R. D.; Minelli, M.; Spence, J. T.; Yamanouchi, K.; Enemark, J. H.; Chasteen, N. D. *Inorg. Chem.* 1979, 18, 3213.

(7) Bishop, P. T.; Dilworth, J. R.; Hutchinson, J.; Zubieta, J. A. *J. Chem. Soc., Chem. Commun.* 1982, 1052.

(8) Kaul, B. B.; Enemark, J. H.; Merbs, S. L.; Spence, J. T. *J. Am. Chem. Soc.* 1985, 107, 2885.

(9) Ellis, S. R.; Collison, D.; Garner, C. D.; Clegg, W. *J. Chem. Soc., Chem. Commun.* 1986, 1483.

(10) Dowerah, D.; Spence, J. T.; Singh, R.; Weed, A. G.; Wilson, G. L.; Farchione, F.; Enemark, J. H.; Kristofzski, J.; Bruck, M. *J. Am. Chem. Soc.* 1987, 109, 5655.

(11) Ueyama, N.; Yoshinaga, N.; Kajiwara, A.; Nakamura, A.; Kusunoki, M. *Bull. Chem. Soc. Jpn.* 1991, 64, 2458.

(12) Chang, C. S. J.; Collison, D.; Mabbs, F. E.; Enemark, J. H. *Inorg. Chem.* 1990, 29, 2261.

(13) Sanz, V.; Picher, T.; Palanca, P.; Gomez-Romero, P.; Llopis, E.; Ramirez, J. A.; Beltran, D.; Cervilla, A. *Inorg. Chem.* 1991, 30, 3113.

(14) Cleland, W. E. J.; Barnhart, K. M.; Yamanouchi, K.; Collison, D.; Mabbs, F. E.; Ortega, R. B.; Enemark, J. H. *Inorg. Chem.* 1987, 26, 1017.

(15) Pickett, C.; Kumar, S.; Vella, P. A.; Zubieta, J. *Inorg. Chem.* 1982, 21, 908.

(16) Boyde, S.; Ellis, S. R.; Garner, C. D.; Clegg, W. *J. Chem. Soc., Chem. Commun.* 1986, 1541.